Results in Physics 16 (2020) 102871

Contents lists available at ScienceDirect

Results in Physics

journal homepage: www.elsevier.com/locate/rinp

A sensitive temperature probe based on Er^{3+}-doped GeO_x films

A.R. Zanatta

Instituto de Física de São Carlos, USP, São Carlos, 13560-970 – SP, Brazil

ARTICLE INFO

Keywords:
Optical sensing
Luminescence
Er-doped
Oxide materials (GeO_x)

ABSTRACT

The light emission due to Er^{3+} ions when inserted in a GeO_x film was analyzed at different temperatures. The film was prepared by sputtering a combined Ge + Er solid target and the incorporation of oxygen took place by thermal annealing the film under a continuous flow of O_2. According to the experimental results, the Er^{3+}-related $^2H_{11/2} \rightarrow {}^4I_{15/2}$ and $^4S_{3/2} \rightarrow {}^4I_{15/2}$ optical transitions – corresponding to the green region of the visible spectrum of electromagnetic radiation – were highly influenced by the local temperature. Compared with other Er^{3+}-doped materials, the present GeO_x:Er film exhibited a rather large $^2H_{11/2}$-to-$^4S_{3/2}$ energy levels separation, suggesting its potential to act as a very sensitive temperature probe in the ~300–750 K range. Along with the Er^{3+}-related optical emission characteristics, the atomic composition and structure of the GeO_x:Er film were also investigated in detail.

Introduction

At ambient conditions, crystalline germanium dioxide GeO_2 adopts either the α-quartz-*like* (hexagonal) or the rutile-*like* (tetragonal) atomic structures [1]. Also, GeO_2 is a thermal stable (~1400 K melting point), wide optical bandgap (~6 eV), high dielectric constant (5.6–8.7) material, that presents a refractive index (1.65) slightly higher than that of SiO_2 (1.55) [2]. Accordingly, films of GeO_2 were considered in optical applications ranging from, for example, infrared filters and detectors to waveguides. Special attention has also been given to sub-stoichiometric GeO_2 (or GeO_x) to function as insulating or passivating layers in electronic components, as well as for storage information purposes [3]. Considering the power exerted by the atomic structure–composition onto the properties of the GeO_x films, different methods of preparation has been reviewed, which included: evaporation (e-beam or thermal), sputtering (dc or rf), laser ablation, plasma-assisted, sol–gel etc. [4]. In all of them, the insertion of oxygen came about during the film deposition itself and/or after preparation by means of special sample processing. Some of these features inspired the study of GeO_x films combined with Er, in which case the main focus was the Er^{3+}-related optical emission at ~1540 nm [5,6]. However, in wide-bandgap materials, Er^{3+} ions are known to present well-defined and rather intense optical transitions in the visible region – just as required in applications such as light display devices or temperature sensors [7,8].

The chemical–physical properties of GeO_x allied to the unique optical characteristics of Er^{3+} ions gave rise to this work that is mainly concerned with the production of Er-doped GeO_x films and their visible Er^{3+}-related light emission. Besides, contrary to most of the studies devoted to optical thermometric purposes (*i.e.*, involving the association of Er^{3+}-Yb^{3+} and non-linear up-conversion processes [9,10]) the present Er^{3+}-doped GeO_x films are easy to produce, stable, and very sensitive. The near-infrared light emission due to the Er^{3+} ions, as well as the main compositional-structural aspects of the GeO_x:Er system are also presented and comprehensively discussed in view of the existing literature.

Experimental details

The starting material consisted in one Er-doped Ge film deposited onto a mirror polished crystalline Si substrate. The film was deposited by Ar^+ ion sputtering a Ge target (99.9999% pure, 126 cm^2 of area) partially covered with Er pieces (99.9%, 8 cm^2), so that its final composition was decided by the relative Er-to-Ge target areas and corresponding sputtering yields [11,12]. During deposition, the Si substrate was kept at 125 ± 10 °C and, after 75 min, a 1 μm thick (uniform) film was achieved. Also, a deposition pressure of 1.5×10^{-4} Torr (preceded by a base pressure of 2×10^{-6} Torr), and a 0.8 W cm^{-2} radio frequency (13.56 MHz) power density were adopted. After deposition, the "Er-doped Ge film + Si substrate" set was cut into various pieces of ~1 × 1 cm^2 and annealed under a continuous flow of oxygen gas (99.99% pure), giving rise to the Er-doped GeO_x (or GeO_x:Er) films. The thermal annealing treatments were cumulative, 30 min long, and were carried out at 200, 300, 400, 500, 600, and 700 ± 10 °C.

All GeO_x:Er films − as-deposited (AD) and after thermal annealing (TA) treatments – were investigated by means of energy-dispersive X-ray (EDX), Raman scattering, and photoluminescence (PL) techniques.

https://doi.org/10.1016/j.rinp.2019.102871
Received 14 November 2019; Received in revised form 4 December 2019; Accepted 6 December 2019
Available online 10 December 2019

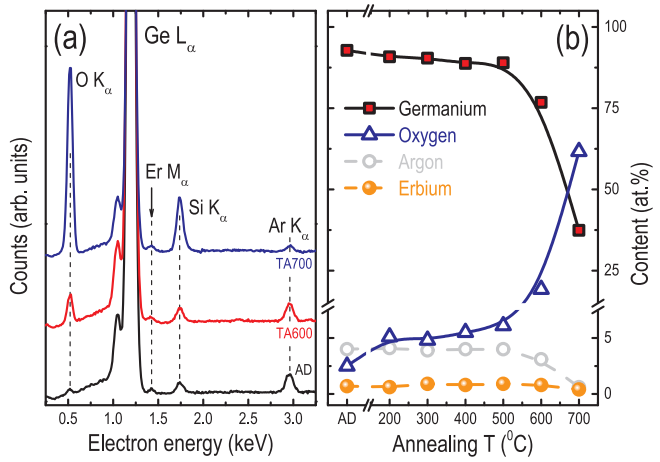

Fig. 1. (a) EDX spectra (15 keV electron energy and 30 × 30 μm^2 analyzed area) of some Er-doped GeO_x films: as-deposited (AD), and after thermal annealing at 600 (TA600) and 700 °C (TA700). The spectra were vertically shifted for clarity reasons. (b) Atomic composition (as determined from the EDX analysis) of the Er-doped GeO_x films, as a function of the annealing temperature. The experimental data error is typically the size of the symbols.

Results and discussion

Composition & structure

As a result of the deposition method and conditions, the GeO_x:Er films presented ~0.5 at.% of Er and oxygen concentrations that scaled with the annealing temperature. The EDX spectra also indicated the presence of some embedded argon atoms (ranging from ~4 to 1 at.%) and the contribution from the Si substrate – this one being more evident owing to the different electron penetration depths in Ge and GeO_x [13]. The EDX spectra and corresponding data analysis are shown in Fig. 1. Based on these results it is clear that all GeO_x:Er films are sub-stoichiometric (*i.e.*, [O] < 66.6 at.%) and, hence, their generic GeO_x designation.

In addition to the compositional changes, thermal annealing at increasing temperatures modified the atomic structure of the films as well. The Raman spectra of Fig. 2(a) show that the as-deposited film is essentially amorphous, as denoted by the broad Ge—Ge scattering signals at: ~85 cm^{-1} (corresponding to the transverse-acoustic TA-*like* phonon mode); ~265 cm^{-1} (transverse-optic TO-*like*); and ~167 and ~230 cm^{-1} (longitudinal- acoustic- and optic-*like* modes, respectively) [14]. The amorphous Ge structure remained up to 700 °C, but after annealing at 600 °C the Raman spectra indicated the presence of crystalline (c-)Ge – as denoted by the well-defined signal at ~300 cm^{-1} (TO) and its overtone at 560 cm^{-1} (2TO) [15].

After treatment at 700 °C, new Raman scattering signals developed – all of them related to crystalline (α-quartz) GeO_2: E(LO + TO) modes at ~120, 160, and 570 cm^{-1}; E(LO) at ~320 cm^{-1}; and A_1 at ~205, 245, and 435 cm^{-1} [16]. A proper way to evaluate these structural changes relies on the analysis of the most intense Raman signals by means of the relative amount (or fraction) of Ge atoms: in the amorphous (TO-*like* mode at 265 cm^{-1}) and crystalline (TO at 300 cm^{-1}) forms, and bonded to oxygen (A_1 at 435 cm^{-1}), for example. These Ge fractions were estimated according to their corresponding Raman signals [17], and are displayed in Fig. 2(b). The results resemble very much those obtained from EDX (Fig. 1) and despite the evident data error (mainly because of the Raman fitting process and related scattering cross-sections) they indicate that, after treatment at 700 °C, the GeO_x:Er film is basically made of ~40% of Ge and ~60% of oxygen. Moreover, temperatures above 500 °C were needed to induce Ge crystallization and the formation of Ge—O bonds.

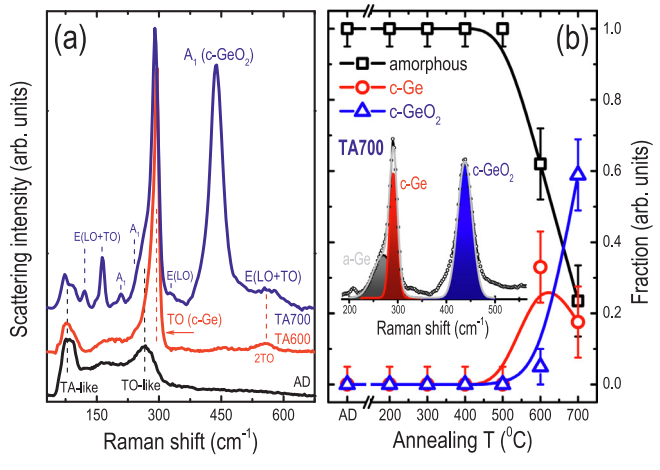

Fig. 2. (a) Room-temperature, non-polarized, Raman scattering spectra (488.0 nm photon excitation) of some Er-doped GeO_x films: as-deposited (AD), and after thermal annealing at 600 and 700 °C. The spectra were vertically shifted for clarity. (b) Fraction of amorphous Ge, c-Ge, and c-GeO_2 Raman signals as the Er-doped GeO_x films were annealed at increasing temperatures. The inset shows the deconvolution of a typical Raman spectrum (sample TA700) illustrating the contributions due to amorphous Ge, c-Ge, and c-GeO_2.

Er^{3+}-related light emission

Traditionally, most of the studies involving the doping of semiconductors with Er^{3+} ions focused on their characteristic near-infrared light emission at ~1540 nm. At this photon wavelength, which coincides with the lowest transmission loss region (*C*-band) of the silica-based optical fibers, the combination of Er^{3+} ions with semiconductor materials was expected to produce great advances in the field of optoelectronics [18]. An interesting outcome of these studies was to verify that the light emission quenching at ~1540 nm tends to occur at higher temperatures in wide-bandgap materials [19], in which case the Er^{3+} ions can also exhibit emission in the visible range [20].

The PL spectra, in the 1450–1675 nm wavelength range, of the GeO_x:Er film annealed at 700 °C are displayed in Fig. 3(a). The measurements were performed at different temperatures and clearly show the $^4I_{13/2} \rightarrow {}^4I_{15/2}$ Er^{3+}-related transition and respective *Stark* splitting

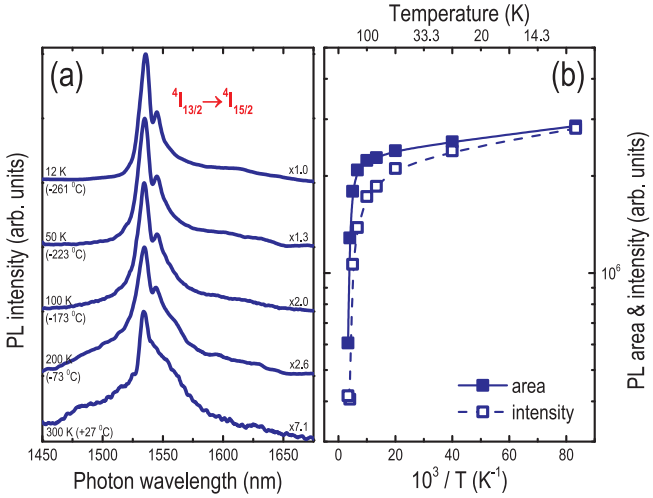

Fig. 3. (a) Photoluminescence spectra (488.0 nm photon excitation) of one Er-doped GeO_x film (TA700) at different temperatures of measurement. The spectra were normalized (see the multiplying factors) and vertically shifted for clarity reasons. (b) PL intensity at 1540 ± 5 nm and PL integrated area (1475–1650 nm range) as a function of the inverse of temperature. PL data error is typically smaller than the size of the symbols.

features around 1540 nm [21]. The influence exerted by the temperature of measurement onto the Er^{3+}-related PL intensity is presented in Fig. 3(b), that also shows the corresponding PL area *i.e.*, PL signal integrated over a predefined spectral band. According to the data, it is clear the almost one order of magnitude variation experienced by the PL signal in the 12–300 K (or −260 to 27 °C) range, and that a very low quenching temperature T_q applies. In fact, $T_q = 25 \pm 5$ K – as defined by the $I_{PL}(T_q) = 0.95\ I_{PL}(T_{lowest})$ variation in the near-infrared PL signal [19] – is perfectly consistent with the presence of Ge—Ge bonds (Fig. 2) in the GeO_x:Er film.

As pointed out by literature, the optical bandgap of GeO_x stays between ~1 eV [22] and 6 eV [23], and it is known to be highly dependent on the deposition conditions and sample processing details that, ultimately, determine the oxygen content and structure of the material [4]. No optical absorption measurements were carried out on the present GeO_x:Er (TA700) film, but based on its atomic composition [Fig. 1(b)] it is reasonable to ascribe an optical bandgap E_{gap} of ~4.5 ± 0.5 eV [24].

Analogous to other Er-doped wide-bandgap materials like GeN (E_{gap} ~ 2.5 eV [7]), TiO_2 (E_{gap} ~ 3 eV [8]), AlN (E_{gap} ~ 4 eV [25]), and SiN (E_{gap} ~ 4.5 eV [26]), in addition to the PL signal at ~1540 nm, the GeO_x:Er film also exhibited light emission in the visible range.

As displayed in Fig. 4(a), one of these Er^{3+}-related emissions took place in the green region of the electromagnetic spectrum and correspond to the $^2H_{11/2} \rightarrow {}^4I_{15/2}$ (at ~525 nm) and $^4S_{3/2} \rightarrow {}^4I_{15/2}$ (at ~550 nm) optical transitions [21]. As can be seen, the transitions exhibit typical *Stark* splitting and, most importantly, their overall shape and intensity were affected by temperature [Fig. 4(b)]. It happens because of the proximity of the $^2H_{11/2}$ and $^4S_{3/2}$ levels such that, depending on the local temperature, electrons can migrate from one level to another [27,28]. More specifically: at higher temperatures electrons recombine preferentially from the upper level at ~525 nm, and *vice-versa*. Part of this phenomenon can be described by an Arrhenius law [Eq. (1)] that relates the PL intensity I_{PL} (or integrated PL area) ratio R(T) of the Er^{3+}-related green transitions and the temperature of measurement. It involves the energy gap between the $^2H_{11/2}$ and $^4S_{3/2}$ levels (Δε), details regarding their degeneracy and emission probability (exponential pre-factor K), and the Boltzmann constant (k_B):

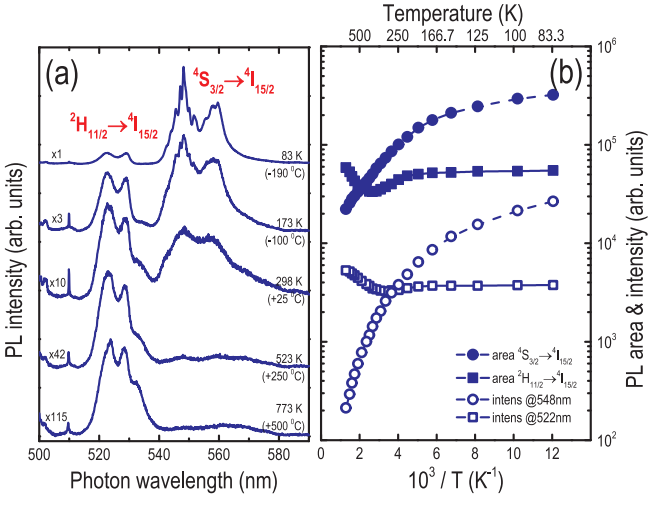

Fig. 4. (a) Photoluminescence spectra (488.0 nm excitation), in the 500–590 nm range, of a GeO_x:Er film (TA700) at different temperatures of measurement. The spectra were normalized (see the multiplying factors) and vertically shifted for clarity. The contribution at ~510 nm (and below) corresponds to the Raman signal due to c-GeO_2. (b) PL intensity (at 525 ± 3 and 550 ± 3 nm) and PL integrated area (515–540 and 540–580 nm range) as a function of the inverse of temperature.

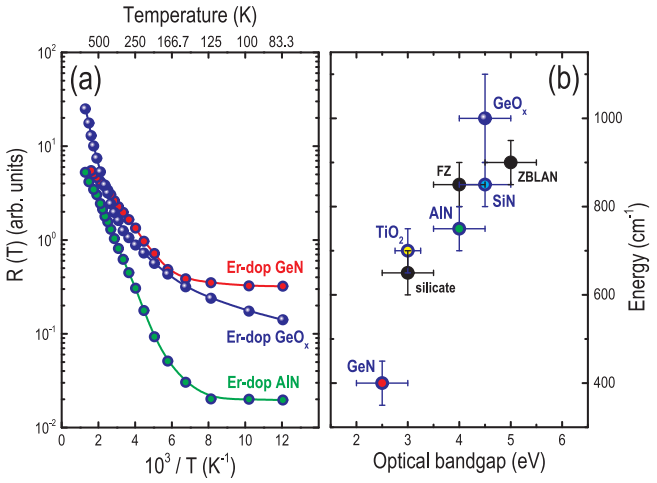

Fig. 5. (a) Photoluminescence intensity ratio R(T) as a function of the inverse of temperature, of Er^{3+}-doped GeN, GeO_x, and AlN films. (b) Energy separation Δε (between the $^2H_{11/2}$ and $^4S_{3/2}$ levels) as a function of the optical bandgap of various Er^{3+}-doped materials: GeN film [7], lead-silicate glass [36], TiO_2 film [8], AlN film [25], fluorozirconate FZ glass [27], SiN film [20,26], ZrF_4-BaF_2-LaF_3-AlF_3-NaF ZBLAN glass [28], and GeO_x film (this work). Error bars comprise both experimental data dispersion and uncertainties from literature.

$$R(T) = \frac{I_{PL}(\,^2H_{11/2} \rightarrow {}^4I_{15/2})}{I_{PL}(\,^4S_{3/2} \rightarrow {}^4I_{15/2})} = K\exp\left(\frac{-\Delta\varepsilon}{k_B T}\right) \quad (1)$$

In spite of its convenience, Eq. (1) considers that all electrons reaching the $^2H_{11/2}$ level originated from the $^4S_{3/2}$ state and ignores other (non-)radiative transition paths [8] – that eventually could be influential at extreme temperatures.

Nonetheless, provided that a calibration curve exists – similar to those presented in Fig. 5(a) – any Er^{3+}-doped wide-bandgap material can be used to efficiently probe the local temperature [29–33]. In this case, the host material will be chosen based on its physical properties and in view of the temperature range of interest. This form the basis of an optically-based temperature sensor, according to which the temperature can be determined, almost instantly, with minimum (or no) physical interference by optical means [34,35]. In common, most of the Er^{3+}-doped materials considered for optical thermometry purposes seem to strictly follow Eq. (1) only above ~150 K, and to present Δε energies that depend on the main characteristics of the host [8,20,26–29,34]. Part of these features are present in Fig. 5: (a) in which a single exponential behavior applies at T ≥ 150 K (or even T > 300 K for the GeO_x:Er film); and (b) that shows the relationship between Δε and the optical bandgap of some Er^{3+}-doped materials. In the former case, other optical excitation–recombination mechanisms can be competing with the Er^{3+}-related green emission and, hence, the different temperature ranges in which Eq. (1) applies. In the latter, the atomic structure–composition leading to wider optical bandgap materials can also be at the origin of larger Δε values [19,29]. At this point, one can only conclude about the influence exerted by the local environment (or crystal field effects) onto the Er^{3+}-related green light emission, and that more research is needed. However, allied to an optical bandgap that can reach ~6 eV, the results of Fig. 5 are very promising, suggesting the suitability of the GeO_x:Er system to act as an efficient optically-based temperature sensor (in the ~300–750 K range).

Concluding remarks

The atomic structure and composition of Er^{3+}-doped GeO_x films were studied by different spectroscopic techniques. The films were prepared by Ar^+ ion sputtering a solid Ge + Er target and, subsequently, thermal annealed under a flow of O_2. Following this approach,

different films were achieved, in which their main properties scaled with the temperature of anneal – ranging from amorphous Ge to sub-stoichiometric crystalline GeO_2 (or c-GeO_x). In all cases, the Er concentration remained in the low 0.5 at.%. The Er^{3+}-related light emission of the film annealed at 700 °C was investigated in detail – both in the near-infrared ($^4I_{13/2} \rightarrow {}^4I_{15/2}$ transition at ~1540 nm) and visible ($^2H_{11/2} \rightarrow {}^4I_{15/2}$ and $^4S_{3/2} \rightarrow {}^4I_{15/2}$ transitions at ~525 and 550 nm) ranges.

According to the experimental results: (1) the originally amorphous Ge films became partially crystallized after annealing above 500 °C; (2) likewise, crystalline Ge−O bonds developed only after treatment at 600 and 700 °C, in which cases the oxygen concentrations reached ~20 and 60 at.%; (3) accordingly, the optical bandgap of the GeO_x:Er TA700 film was anticipated to be around 4.5 ± 0.5 eV; (4) despite such a wide optical bandgap, the T-quenching experienced by the $^4I_{13/2} \rightarrow {}^4I_{15/2}$ near-infrared light emission (at ~1540 nm) is consistent with the presence of Ge−Ge bonds; (5) regarding the Er^{3+}-related emissions taking place in the green visible region ($^2H_{11/2} \rightarrow {}^4I_{15/2}$ and $^4S_{3/2} \rightarrow {}^4I_{15/2}$ transitions), they proved to be highly susceptible to temperature effects, presenting a single exponential behavior in the ~300–750 K range.

Altogether, this work reports the first results involving the Er^{3+}-related green light emissions from the GeO_x:Er system, which is being proposed as a very effective medium for optical thermometric applications.

Declaration of Competing Interest

The authors declare that they have no known competing financial interests or personal relationships that could have appeared to influence the work reported in this paper.

Acknowledgements

This work was financially supported by the Brazilian agencies FAPESP and CNPq.

References

[1] Micoulaut M, Cormier L, Henderson GS. The structure of amorphous, crystalline and liquid GeO_2. J Phys Condens Matter 2006;18:R753–84. https://doi.org/10.1088/0953-8984/18/45/R01.

[2] See, for example, W. J. Tropf, T. J. Harris, M. E. Thomas, Optical materials: Visible and infrared, in Electro-Optics Handbook. Chap. 11, Eds. R. W. Waynant, M. N. Ediger, McGraw-Hill, New York, NY 2000. ISBN 0-07-068716-1.

[3] Murphy NR, Grant JT, Sun L, Jones JG, Jakubiak R, Shutthanandan V, et al. Correlation between optical properties and chemical composition of sputter-deposited germanium oxide (GeO_x) films. Opt Mater 2014;36:1177–82. https://doi.org/10.1016/j.optmat.2014.02.023.

[4] Al-Kuhaili MF, Durrani SMA. Incorporation of oxygen into thermally evaporated germanium and optical characterization of the resulting films. J Appl Phys 2007;102(5):1–5. https://doi.org/10.1063/1.2776007. 053512.

[5] Chen JH, Pang D, Cheong HM, Wickboldt P, Paul W. Room-temperature 1.5 μm luminescence of co-deposited erbium and germanium. Appl Phys Lett 1995;67:2182–4. https://doi.org/10.1063/1.115096.

[6] Ardyanian M, Rinnert H, Vergnat M. 1.54μm photoluminescence of Er-doped GeOx thin films. J Appl Phys 2007;102(10):1–3. https://doi.org/10.1063/1.2811725. 106103.

[7] Zanatta AR, Ribeiro CTM. Laser-induced generation of micrometer-sized luminescent patterns on rare-earth-doped amorphous films. J Appl Phys 2004;96:5977–81. https://doi.org/10.1063/1.1794363.

[8] Scoca D, Morales M, Merlo R, Alvarez F, Zanatta AR. Photoluminescence and compositional-structural properties of ion-beam sputter deposited Er-doped $TiO_{2-x}N_x$ films: their potential as a temperature sensor. J Appl Phys 2015;117:1–6. https://doi.org/10.1063/1.4921809. 205304.

[9] Cai Y, Feng S, Ming C, Ren X, Qin Y, An L. Researching on thermal characters in Yb^{3+}/Er^{3+} codoped phosphate glass ceramic for fluorescence temperature sensor. Res Phys 2016;6:826–8. https://doi.org/10.1016/j.rinp.2016.09.009.

[10] Lia Y, Chena B, Tonga L, Zhanga X, Xua S, Lia X, Zhanga J, Suna J, Wanga X, Zhanga Y, Suia G, Zhanga Y, Zhanga X, Xiab H. A temperature self-monitoring $NaYF_4:Dy^{3+}/Yb^{3+}$@$NaYF_4:Er^{3+}/Yb^{3+}$ coreshell photothermal converter for photothermal therapy application. Res Phys 2019;15:1–7. https://doi.org/10.1016/j.rinp.2019.102704. 102704.

[11] Vossen JL, Cuomo JJ. Glow discharge sputter deposition. In: Vossen JL, Kern W, editors. Thin-Film Processes. New York, NY: Academic Press Inc.; 1978. Chap. II-1, eBook ISBN: 9780323138987.

[12] Zanatta AR, Ribeiro CTM, Alvarez F. X-ray photoelectron spectroscopic study of rare-earth-doped amorphous silicon-nitrogen films. J Appl Phys 2003;93:1948–53. https://doi.org/10.1063/1.1536015.

[13] See, for example Yacobi BG, Holt DB. Cathodoluminescence scanning electron microscopy of semiconductors. J Appl Phys 1986;59:R1–24. https://doi.org/10.1063/1.336491.

[14] Bermejo D, Cardona M. Raman scattering in pure and hydrogenated amorphous germanium and silicon. J Non-Crystal Sol 1979;32:405–19. https://doi.org/10.1016/0022-3093(79)90085-1.

[15] Parker JH, Feldman DW, Ashkin M. Raman scattering by silicon and germanium. Phys Rev 1967;155:712–4. https://doi.org/10.1103/PhysRev. 155.712.

[16] Scott JF. Raman spectra of GeO_2. Phys Rev B 1970;1:3488–93. https://doi.org/10.1103/PhysRevB.1.3488.

[17] Zanatta AR, Ferri F. Metal-induced crystallization by homogeneous insertion of metallic species in amorphous semiconductors. In: Wang Z, Jeurgens L, Mittemeijer E, editors. Metal-Induced Crystallization: Fundamentals & Applications. Boca Raton, FL: CRC Press; 2015 Chapter 4, ISBN 9789814463409.

[18] Kenyon AJ. Recent developments in rare-earth doped materials for optoelectronics. Prog Quantum Electron 2002;26:225–84. https://doi.org/10.1016/S0079-6727(02)00014-9.

[19] Zanatta AR. Photoluminescence quenching in Er-doped compounds. Appl Phys Lett 2003;82:1395–7. https://doi.org/10.1063/1.1557318.

[20] Zanatta AR, Nunes L. Green photoluminescence from Er-containing amorphous SiN thin films. Appl Phys Lett 1998;72:3127–9. https://doi.org/10.1063/1.121568.

[21] Dieke GH. Spectra and energy levels of rare-earth ions in crystals. New York, NY: Interscience Pub; 1968.

[22] Shabalov AL, Feldman MS. Optical properties of thin GeO_x films. Phys Stat Sol (a) 1984;83:K11–4. https://doi.org/10.1002/pssa.2210830151.

[23] Lange T, Njoroge W, Weis H, Beckers M, Wuttig M. Physical properties of thin GeO_2 films produced by reactive DC magnetron sputtering. Thin Sol Films 2000;365:82–9. https://doi.org/10.1016/S0040-6090(99)01106-2.

[24] Aita CR, Marhic ME, Sayers CN. Near-ultraviolet-visible, near-infrared optical behavior of sputter deposited GeO_x. Defect Diffus Forum 1987;53–54:55–60. https://doi.org/10.4028/www.scientific.net/DDF.53-54.55.

[25] Zanatta AR, Ribeiro CTM, Jahn U. Optoelectronic and structural characteristics of Er-doped amorphous AlN films. J Appl Phys 2005;98(1–8):1–8. https://doi.org/10.1063/1.2127120. 093514.

[26] Zanatta AR, Bell M, Nunes L. Visible photoluminescence from Er^{3+} ions in a-SiN alloys. Phys Rev B 1999;59:10091–8. https://doi.org/10.1103/PhysRevB.59.10091.

[27] Shinn MD, Sibley WA, Drexhage MG, Brown RN. Er^{3+} ions in fluorozirconate glass. Phys Rev B 1983;27:6635–48. https://doi.org/10.1103/PhysRevB.27.6635.

[28] Yokokawa T, Inokuma H, Ohki Y. Nature of photoluminescence involving transitions from the ground to $4f^{n-1}$ $5d^1$ states in rare-earth-doped glasses. J Appl Phys 1995;77:4013–7. https://doi.org/10.1063/1.359530.

[29] Collins SF, Baxter GW, Wade SA, Sun T, Grattan KTV, Zhang ZY, et al. Comparison of fluorescence-based temperature sensor schemes: Theoretical analysis and experimental validation. J Appl Phys 1998;84:4649–54. https://doi.org/10.1063/1.368705.

[30] Chen J, Zhao JX. Upconversion nanomaterials: synthesis, mechanism, and applications in sensing. Sensors 2012;12:2414–35. https://doi.org/10.3390/s120302414.

[31] Zhenga H, Chena B, Yub H, Lia X, Zhanga J, Suna J, et al. Rod-shaped $NaY(MoO_4)_2:Sm^{3+}/Yb^{3+}$ nanoheaters for photothermalconversion: Influence of doping concentration and excitation power density. Sens Act B Chem 2016;234:286–93. https://doi.org/10.1016/j.snb.2016.04.162.

[32] Tong L, Li X, Zhang J, Xu S, Sun J, Zheng H, et al. $NaYF_4:Sm^{3+}/Yb^{3+}$@$NaYF_4:Er^{3+}/Yb^{3+}$ core-shell structured nanocalorifier with optical temperature probe. Opt Exp 2017;25:16047–58. https://doi.org/10.1364/OE.25.016047.

[33] Zhang Y, Su X, Li X, Zhang J, Sun J, Xia H, et al. Temperature sensing, excitation power dependent fluorescence branching ratios, and photothermal conversion in $NaYF_4:Er^{3+}/Yb^{3+}$@$NaYF_4:Tm^{3+}/Yb^{3+}$ core-shell particles. Opt Mater Exp 2018;8:368–84. https://doi.org/10.1364/OME.8.000368.

[34] Wade SA, Collins SF, Baxter GW. Fluorescence intensity ratio technique for optical fiber point temperature sensing. J Appl Phys 2003;94:4743–56. https://doi.org/10.1063/1.1606526.

[35] Brites CDS, Lima PP, Silva NJO, Millán A, Amaral VS, Palacio F, et al. Thermometry at the nanoscale. Nanoscale 2012;4:4799–829. https://doi.org/10.1039/C2NR30663H.

[36] Capobianco JA, Prevost G, Proulx PP, Kabro P, Bettinelli M. Upconversion properties of Er^{3+} doped lead silicate glasses. Opt Mater 1996;6:175–84. https://doi.org/10.1016/0925-3467(96)00031-6.